

Potential Limitations of Bioluminescent Xenograft Mouse Models: A Systematic Review

Yen Ting Shen¹, Rashi Asthana¹, Casper Peeters², Christine Allen¹, Carlo DeAngelis¹, Micheline Piquette-Miller¹

¹Department of Pharmaceutical Sciences, Leslie Dan Faculty of Pharmacy, University of Toronto, Toronto, ON, Canada; ²Imaging Department, University Medical Centre, Utrecht, The Netherlands.

Received, February 24, 2020; Accepted, May 9, 2020; Published, May 10, 2020.

ABSTRACT - PURPOSE: Bioluminescent imaging (BLI) is a versatile technique that offers non-invasive and real-time monitoring of tumor development in preclinical cancer research. However, the technique may be limited by several factors that can lead to misinterpretation of the data. This review aimed to investigate the validity of current BLI tumor models and provide recommendations for future model development. **METHODS:** Two major databases, MedLine and EMBASE, were searched from inception to July 2018 inclusively. Studies utilizing mouse xenograft models with demonstration of linear correlations between bioluminescent signal and tumor burden were included. Coefficients of correlation and determination were extracted along with data relating to animal model parameters. **RESULTS:** 116 studies were included for analysis. It was found that the majority of models demonstrate good correlation regardless of the model type. Selection of a single cell clone with highest luciferase expression resulted in a significantly better correlation. Lastly, appropriate tumor measurement techniques should be utilized when validating the BLI model. **CONCLUSIONS:** In general, BLI remains a valid tool for pre-clinical assessment of tumor burden. While no single factor may be identified as a general limitation, data should be interpreted with caution.

INTRODUCTION

Optical imaging techniques have become a powerful tool in cancer research by providing a means of non-invasive tumor monitoring (1). In comparison to current imaging methods, bioluminescent imaging (BLI) is becoming increasingly popular for researchers due to its high signal-to-noise ratio, rapid image acquisition, and relative ease in technical operation (2). In addition, the principle of light generation from live cells makes BLI highly specific to xenografts developed from luciferase transfected cells; several studies have shown that BLI correlates well with tumor burden (3,4). As such, BLI has been commonly employed as a method of tracking tumor growth and assessing treatment efficacy in preclinical models (5–7).

Despite its versatility, many factors exist that could impact the validity of BLI in preclinical tumor model monitoring (8). For instance, the intrinsic properties of tumor microenvironments such as necrosis and hypoxia can decrease light output leading to inaccurate interpretation of data (8). In a study by Tuli *et al.*, a plateau of bioluminescent signal was observed with large, necrotic tumors when approaching the study end point (9). Another study also demonstrated a poor correlation between

BLI signal and tumor burden when tumor size exceeded 1.2 cm (10). Additionally, the route of luciferin administration may also affect signal intensity due to differences in substrate availability (11). For instance, peak signal intensity, optimal time of imaging, and the duration of the signal has been found to vary depending on the location of the tumor and the route of substrate delivery (12). Lastly, tumor models that generate ascites could also be susceptible to decreases in photon emission due to signal quenching by the fluid (13). Therefore, while BLI tumor monitoring has the potential to accelerate the assessment of drug efficacy and provide data that are normally not available from traditional models, these factors must be considered when utilizing this technique. Indeed, in a study validating a bioluminescent model of breast cancer, different efficacy outcomes were observed between orthotopic and intraperitoneal models (14). Importantly, although BLI correlates well with tumor burden in subcutaneous models, the correlation is reportedly reduced in disseminated intraperitoneal tumor models (5).

Corresponding Author: Prof. Micheline Piquette-Miller, m.piquette.miller@utoronto.ca; 144 College St. Toronto, Ontario, Canada, M5S 3M2, ORCID: 0000-0002-3847-8224

While subcutaneous xenografts are relatively easy to establish, they do not recapitulate normal pathophysiological conditions of cancer as most tumors in the clinic arise within the body cavity. As such, orthotopic or intraperitoneal xenograft models have become increasingly popular due to their ability to better represent clinically relevant disease conditions.

Based on these reported limitations and the widespread use of BLI in preclinical tumor models, it is imperative to better understand and validate the use of BLI as a tool for assessing tumor burden. In the present review, we performed a systematic literature search to identify studies that have utilized BLI in mice xenograft model. The values of correlation of determination (R^2) for eligible publications were extracted to determine the primary limitations and the extent to which these factors impact the validity of the model.

METHODS

Study Design

The protocol for the present systematic review was conducted and documented in accordance to the Preferred Reporting Items for Systematic Reviews and Meta-Analysis (PRISMA) guidelines.

Search Strategy

The aim of this search was to include articles reporting correlations between *in vivo* bioluminescence signal and tumor burden in mouse models. Two authors (YS and CP) independently searched two databases (MedLine and EMBASE) from inception to July 2018 with publications limited to English language. Four sets of search terms were combined with “AND”. The first set consists of terms related to bioluminescence; the second set contains words describing cancer, xenografts, and peritoneal establishment; the third set includes synonyms of mouse; and the last set were keywords describing the outcome of measure. Terms within each set were combined with “OR”. The complete search strategy is shown in **Suppl. Table 1**. Reference lists from relevant review articles were also searched and are summarized as “other sources” in the PRISMA flow chart (**Figure 1**).

Selection Criteria

Eligibility of all identified records was screened by two independent reviewers (YS and CP). Titles and abstracts were searched for a combination of

keywords included in the complete search terms. Full articles were retrieved and screened if inclusion was unable to be determined by title and abstract. Publications were included if they met the following criteria: 1) primary research articles using mouse tumor models; 2) tumor progression or tumor response to treatment monitored by luciferase-based bioluminescent imaging; 3) examined linear correlation between bioluminescent signal and tumor volume or tumor weight measured by caliper or other imaging modalities. Review articles were excluded. Publications were also excluded if the research was conducted in rats, if tumors were monitored using fluorescence or other luminescence techniques, or if non-linear correlations were performed to evaluate the relationship between tumor burden and bioluminescence.

Data Extraction and Analysis

Data was extracted independently by three authors (YS, CP, and RA). Values of coefficient of correlation (R) or coefficient of determination (R^2) between bioluminescent signal and tumor burden were extracted. When possible, details pertaining to types of cancer cell lines, location of xenograft, disease state, methods of tumor burden assessment and number of animals used were obtained. In addition, parameters associated with the BLI technique including selection of single cell clones after transfection or transduction, type of luciferase utilized, and route of substrate administration were also recorded. Linear regression analyses were performed using STATA (version 15, College Station, TX, USA) to determine the association between R^2 values and parameters of the tumor model. For publications that reported only R values, R^2 were obtained by squaring the respective R values. A p value < 0.05 was considered statistically significant for all analyses. R^2 values obtained from intravenous (i.v) and orthotopic (o.t.) models were grouped in analysis between correlation and tumor inoculation site. Additionally, R^2 values obtained in models measured by *ex vivo* BLI and fluorescence-activated cell sorting (FACS) were grouped in the regression analysis between R^2 and tumor assessment methods. R^2 values obtained from spontaneous transgenic models were not included in the regression analysis due to a small sample size.

RESULTS

Characteristics of Studies

From the two databases and other sources, 7,874 records were identified (**Figure 1**). Of them, 2,024 were duplicates. A total of 5,850 records were included for initial title and abstract screening. 1,374 articles were excluded for clear lack of fit with our eligibility criteria. 2,606 conference abstracts were screened and subsequently excluded due to ineligibility. The remaining 1,870 articles were subject to full text screening and 1,754 records were excluded for reasons including no correlation reported ($n=1,422$), lack of relevance to our objective ($n=236$), correlation reported only for *in vitro* study ($n=87$), and relationship was determined

through non-linear correlation ($n=9$). A final sample of 116 articles was included. Of the included articles, 12 reported on two different models, resulting in a total number of models included in the review to be 128. Of all the reported models, 37.5% (48/128) were subcutaneous (s.c) models, 11.7% (15/128) were intraperitoneal (i.p) models or o.t. models that resulted in peritoneal tumors, 41.4% (53/128) were o.t. models that resulted in tumors outside of the peritoneal cavity, and 9.4% (12/128) were i.v. or spontaneous transgenic mouse models. A majority of the models established solid tumors (70.3%, 90/128) whereas disseminated disease was observed in 38 models (29.7%). A total of 207 correlations were extracted from 116 articles.

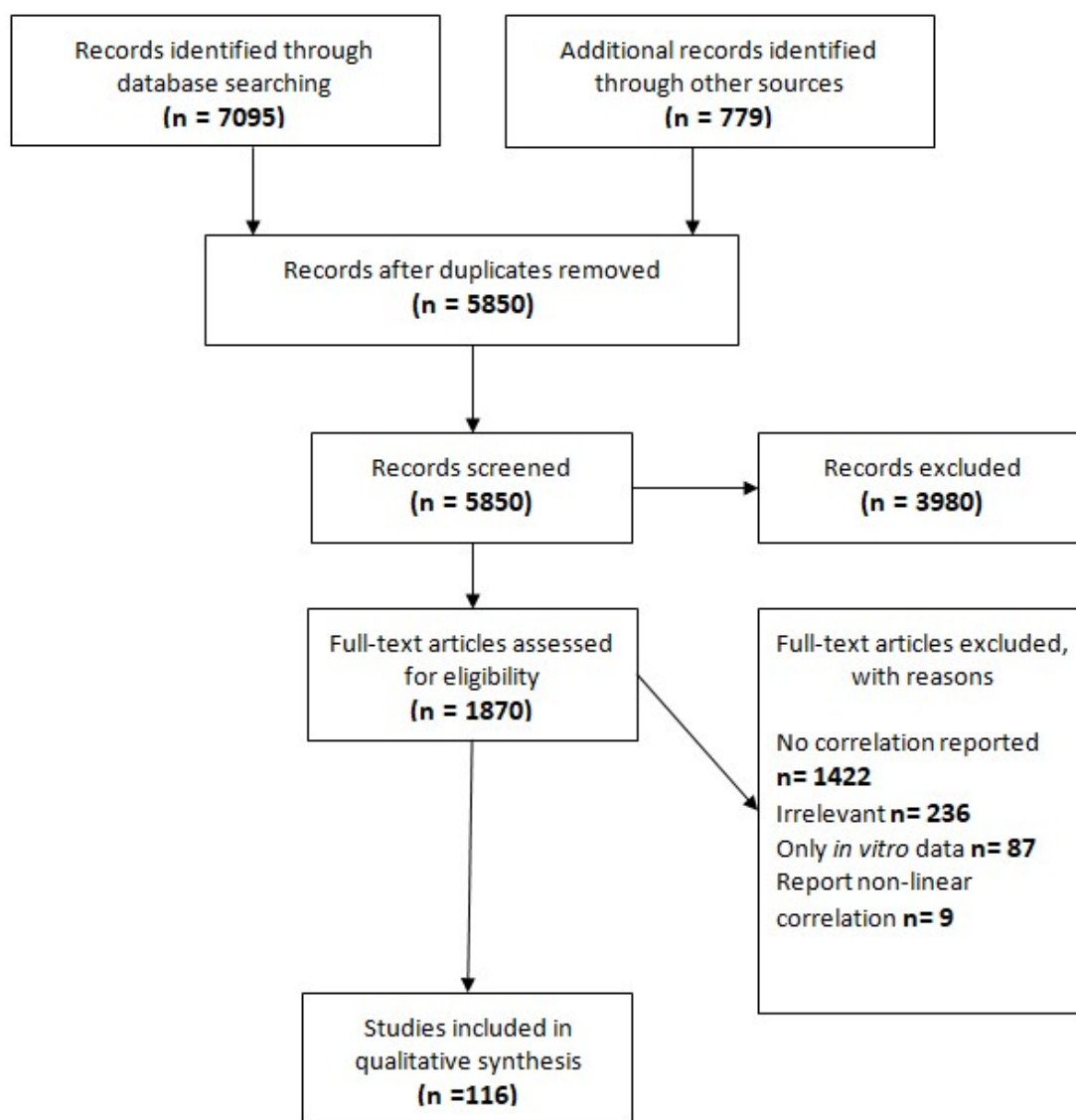


Figure 1. PRISMA flow chart outlining the process of study assessment and selection

Correlation between BLI and Tumor Burden in Models with Different Inoculation Sites

It has been shown that BLI correlates well with tumor burden in s.c. models due to the ease of tumor assessment. Conversely, xenografts that grow inside the body cavity, such as in intraperitoneal or orthotopic models, may result in signal attenuation and poor correlations. Therefore, we first investigated whether the validity of BLI is impacted by different models of tumor origin. Linear regression analysis suggested that no relationship exists between R^2 and different types of tumor model ($p=0.6642$). The median R^2 values (**Figure 2**) were 0.86, 0.80, 0.80, 0.87 and 0.79 for subcutaneous, intraperitoneal, orthotopic, intravenous and transgenic models, respectively. The proportion of R^2 value over 0.5 for s.c, i.p, and o.t models were

82% (65/79), 76% (19/25) and 87% (77/89), respectively.

Effect of Luciferase Expression on Correlation

The generation of luciferase-expressing cells is the foundation of BLI xenograft models. We therefore evaluated the impact of luciferase expression on the correlation of BLI and tumor burden. Our regression model revealed that a better correlation is associated with tumor models developed using the highest luciferase expressing cell population, obtained through means of clonal selection ($p<0.05$). Specifically, the regression predicts a decrease of 0.1 in R^2 value for models that do not utilize clonally selected cells. In addition, less variability was also observed for the clonally selected models as shown by a narrower interquartile range (**Figure 3**).

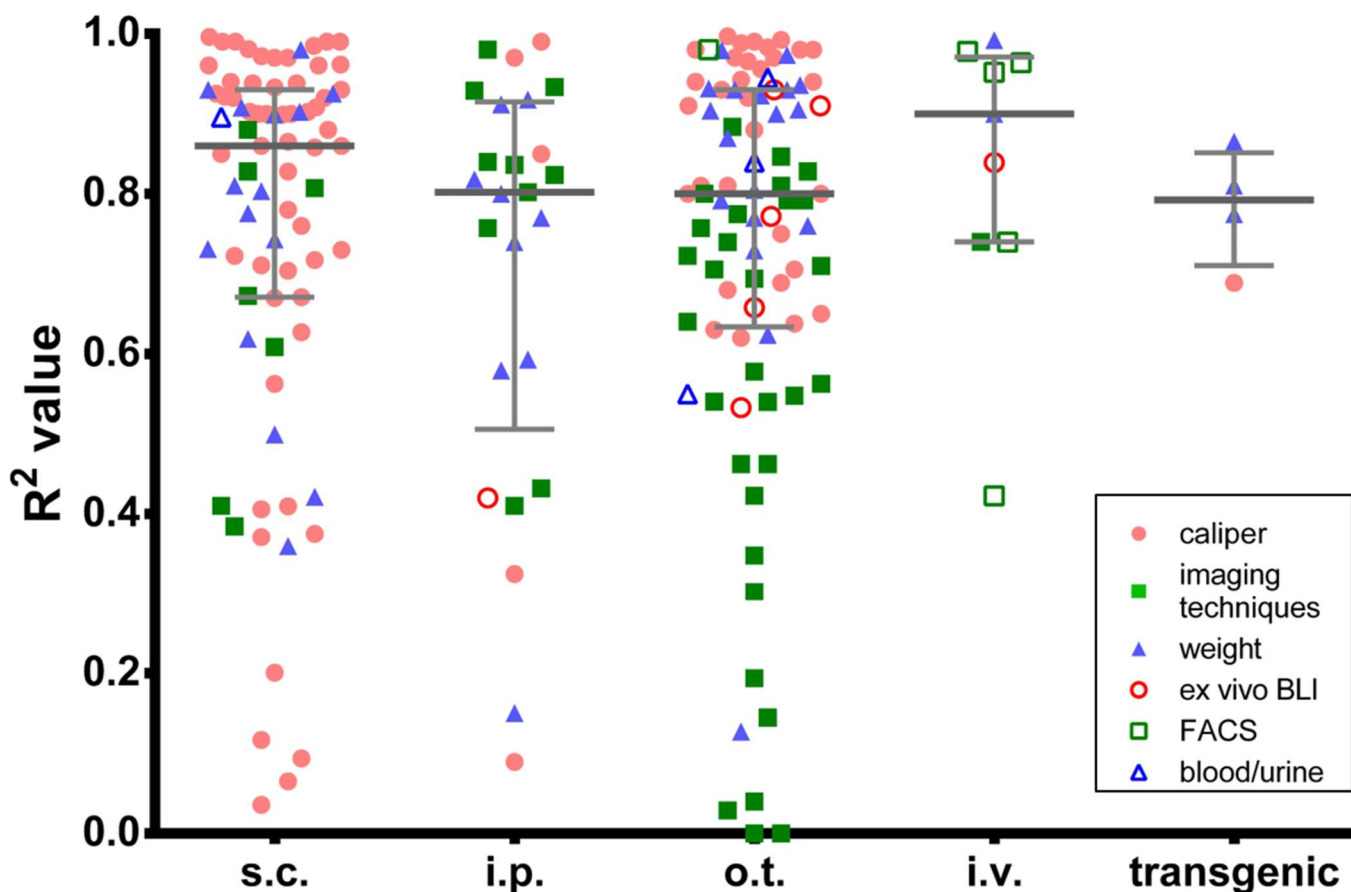


Figure 2 Median R^2 values for correlation obtained between bioluminescence signal and tumor burden in models of distinct tumor origins: subcutaneous (s.c), intraperitoneal (i.p), orthotopic (o.t), intravenous (i.v). Figure legend denotes the method used to determine tumor burden: tumor volume as measured by caliper (red dot); tumor volume as measured by imaging techniques including CT, MRI, PET and ultrasound (green solid rectangle); total weight of tumor nodule(s) (blue solid triangle); BLI signal of the excised nodule(s) (red circle); percentage of BLI positive tumor cells by fluorescent activated cell sorting (green rectangle); BLI signal in blood or urine (blue triangle). Median and interquartile range are indicated on the scatter plot.

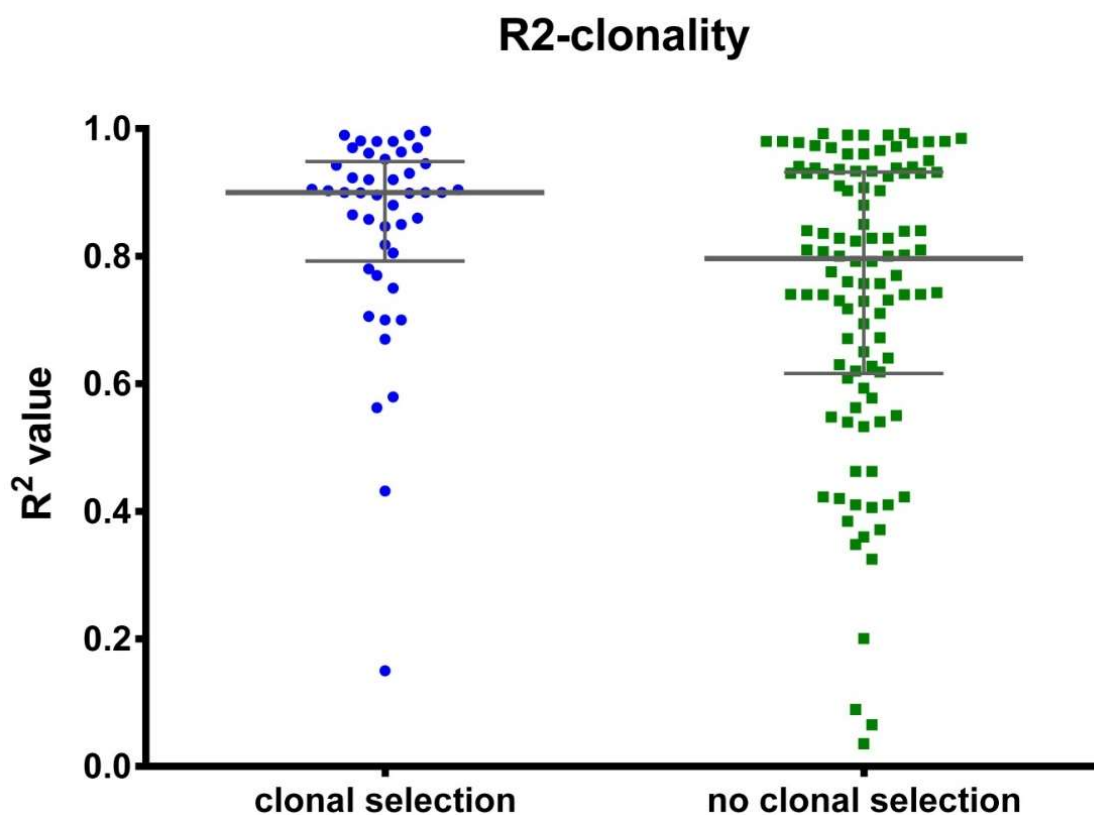


Figure 3. Models derived from clonally-selected cell populations demonstrated an improved correlation between bioluminescent signal correlation and tumor burden.

Effect of Tumor Burden Assessment Method on Correlation

In xenograft mouse models, several techniques may be used to assess tumor burden post-mortem. As such, the method of tumor assessment and its impact on the correlation with BLI was examined. Overall, the correlation between BLI and tumor burden when measured using different tumor assessments remained strong with median R^2 values ranging from 0.72 to 0.92 (**Figure 4**). Despite this, tremendous variability was observed as demonstrated by the wide distribution of R^2 values across the methods of tumor burden assessment. Interestingly, the regression model demonstrated a significant negative relationship between R^2 and measuring tumor by non-BLI imaging-based techniques ($p < 0.0001$). Indeed, the correlation with BLI data was the lowest (median $R^2 = 0.71$) when non-BLI imaging techniques (MRI/CT/PET/Ultrasound) were used to assess tumor burden as compared to the traditional methods for evaluating tumor burden (*i.e.* using calipers and tumor weight). To further our analysis, we grouped each model based on the methods of tumor burden measurement (*i.e.* by

calipers, tumor weight, or non-BLI imaging-based techniques) and evaluated the impact of tumor location (s.c., i.p. or o.t.) and disease presentation (solid or disseminated tumor) on the R^2 values. In models measuring tumor burden by caliper, no relationship was found between R^2 and tumor origin ($p = 0.0654$). Similarly, no association was established when these models were categorized into solid tumor ($p = 0.2167$). Comparison between models in disseminated disease was not done due to small sample size in both s.c. and i.p. groups ($n = 3$ and $n = 2$ for s.c. and i.p. models, respectively). Nonetheless, all three models produced good correlations, however high variability was found in i.p. models (**Figure 5**). In contrast, in solid tumors, BLI positively correlates with tumor burden by weight in o.t. models ($p < 0.05$). However, no relationship was found in disseminated tumors regardless of the model type ($p = 0.9236$) (**Figure 6**). Interestingly, the regression analysis demonstrated significant positive correlation between R^2 and non-BLI imaging techniques in i.p. models, regardless of whether the disease was presented as a solid tumor or a disseminated pattern ($p < 0.05$) (**Figure 7**).

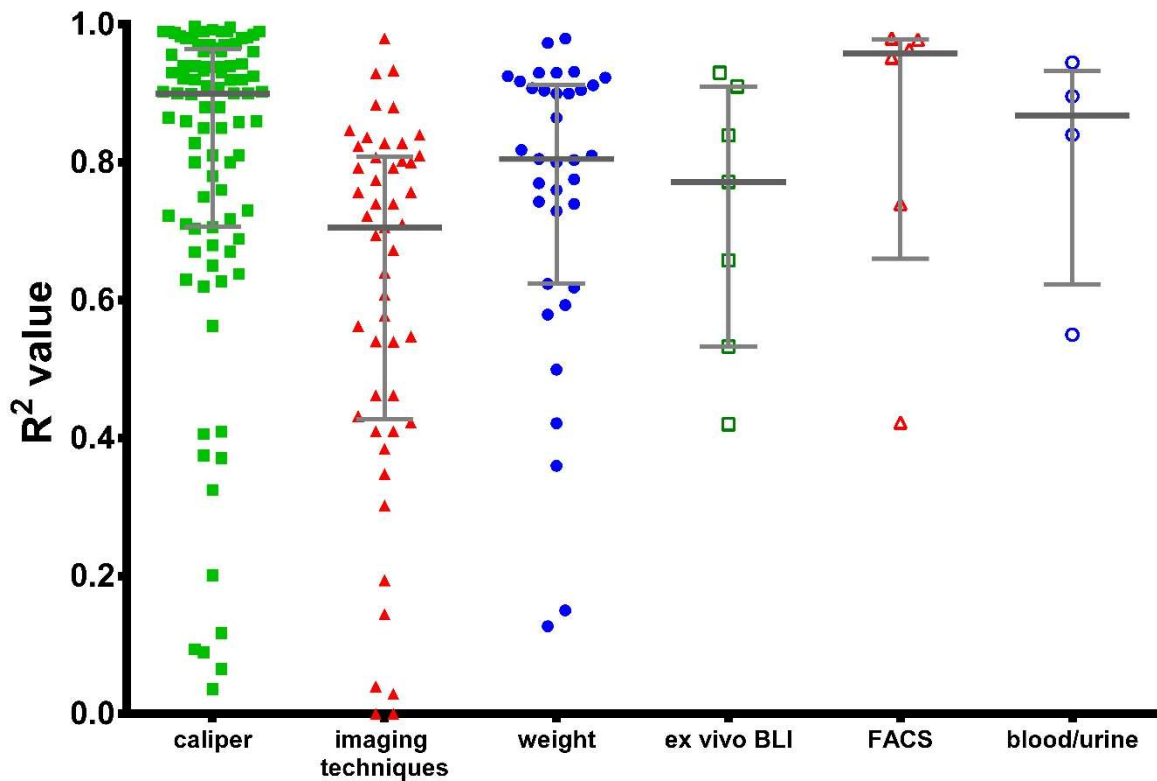


Figure 4 Median R^2 values for correlation obtained between tumor burden measured using bioluminescence signal and tumor burden measured using various techniques, including CT, MRI, PET or ultrasound; BLI: bioluminescence imaging; FACS: fluorescent-activated cell sorting. Median and interquartile range are indicated on the scatter plot.

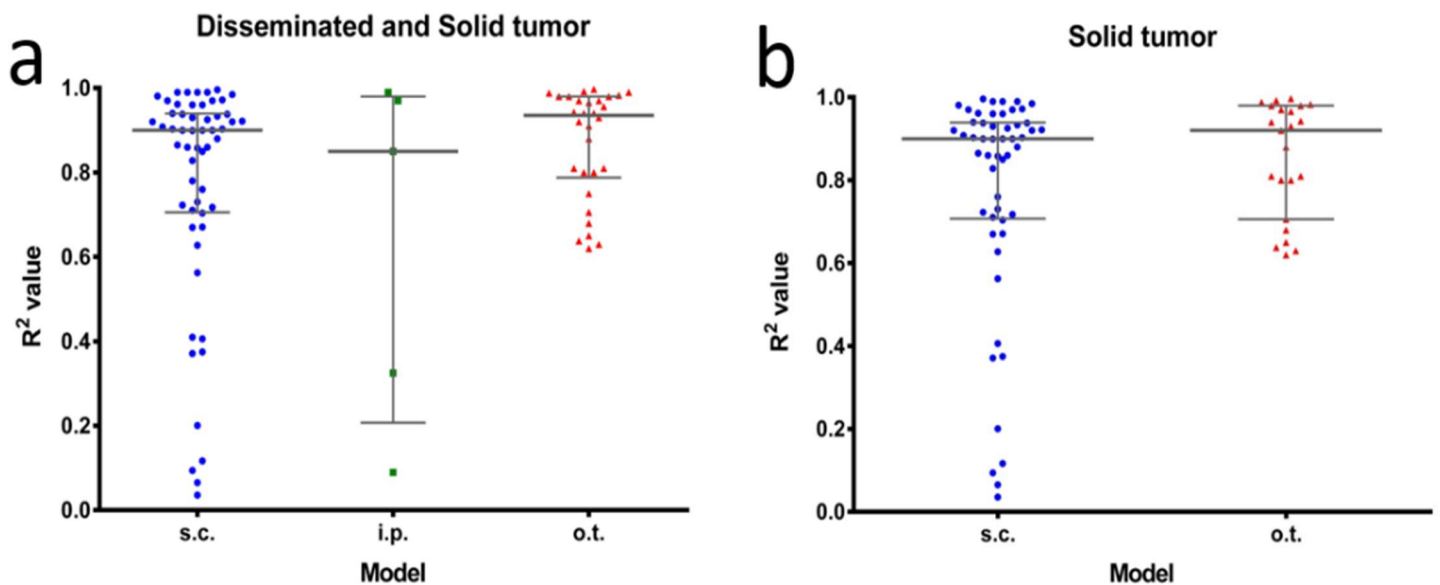


Figure 5 The correlation between tumor burden measured using bioluminescence signal and tumor burden measured using calipers in subcutaneous (s.c.), intraperitoneal (i.p.) and orthotopic (o.t.) models in **a) solid tumor and disseminated disease**, **b) solid tumor alone**; i.p. models were removed from analysis due to small sample size (n=3). Median and interquartile range are indicated on the scatter plot.

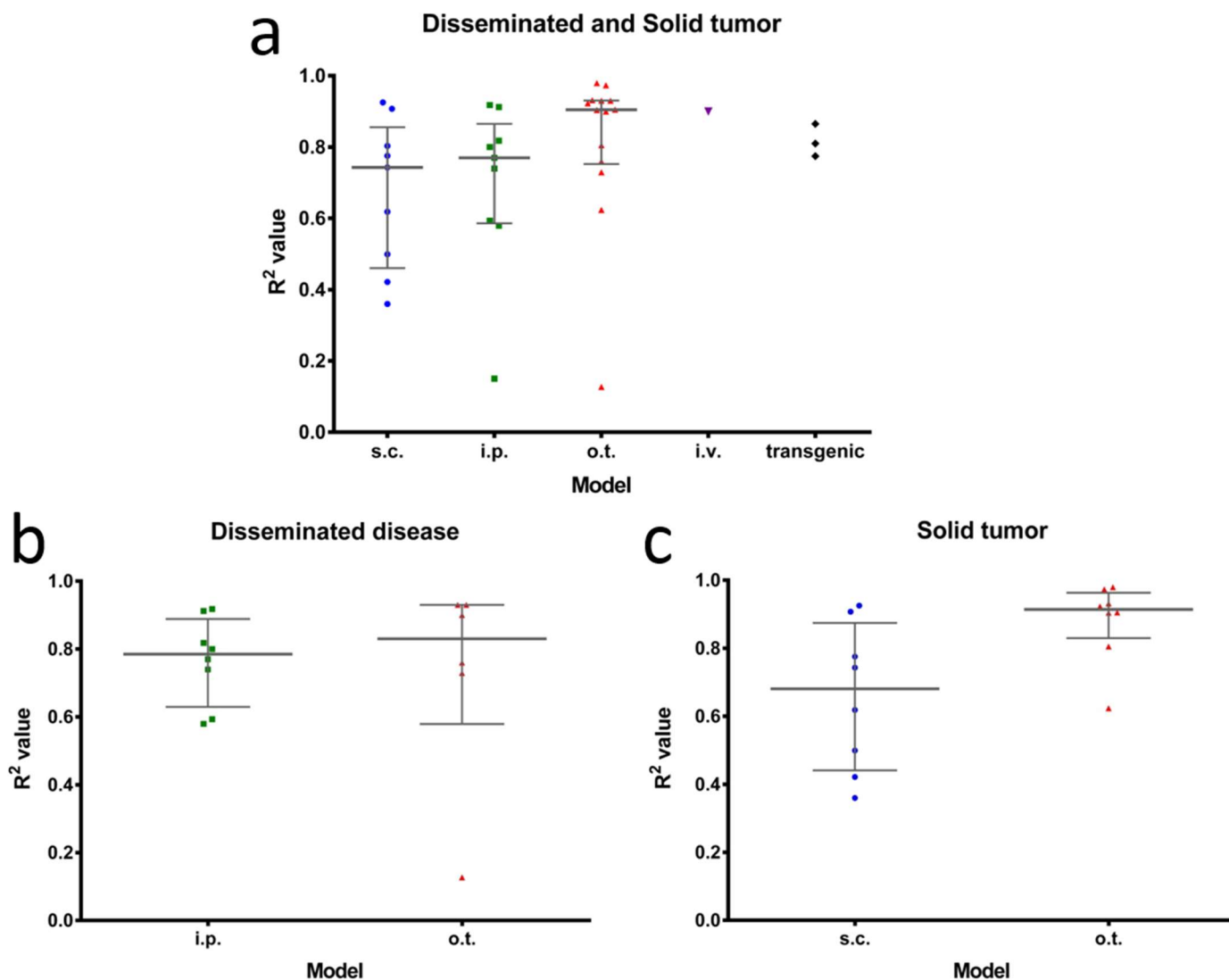


Figure 6 The correlation between tumor burden measured using bioluminescence signal and tumor burden measured using the weight of tumor nodule(s) in subcutaneous (s.c.), intraperitoneal (i.p.), orthotopic (o.t.), intravenous (i.v.) and spontaneous transgenic models in **a) solid tumor and disseminated disease; b) disseminated disease alone; And c) solid tumor alone**; several models were removed from the graphical presentation and analysis due to small sample size ($n \leq 3$). Median and interquartile range are indicated on the scatter plot.

DISCUSSION

Owing to its high sensitivity and ability to distinguish between live and dead cells, BLI has become a popular method for evaluating treatment response in xenograft models. While individual research groups validated their models before proceeding to treatment evaluation, there are contradictory results reported in the literature on the correlation between tumor burden as determined by BLI and other techniques (5). In this review, we have systematically searched two major databases from inception to July 2018 for publications that have

reported correlations between BLI and tumor burden in xenograft mouse models. It was demonstrated that despite variabilities, BLI generally correlated strongly to tumor burden. Moderate to good correlations were observed for various methods of tumor assessment. BLI measurements were well correlated for solid tumors measured by caliper, with tumor burden measured by weight in o.t. models, and for non-BLI imaging-based tumor measurements in i.p. xenografts. Importantly, selecting single cell populations with the highest luciferase expression improved the correlation between BLI and tumor burden.

Disseminated and Solid tumor

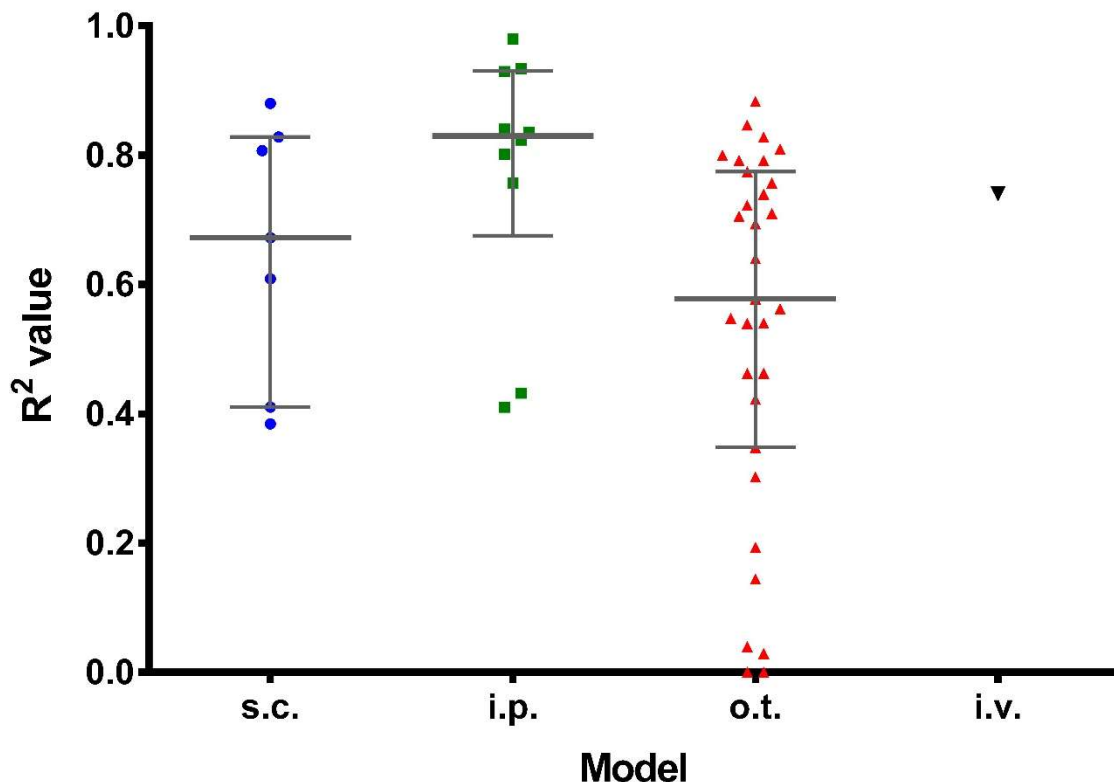


Figure 7 The correlation between tumor burden measured using bioluminescence signal and tumor burden measured using non-BLI imaging-based techniques in subcutaneous (s.c.), intraperitoneal (i.p.), orthotopic (o.t.), and intravenous (i.v.) models with either a solid tumor or a disseminated disease, i.v. model was removed from analysis due to small sample size (n=1), but was included in the figure for complete presentation of data. Median and interquartile range are indicated on the scatter plot.

Light generation from luciferase is highly specific to living cells due to the requirement of ATP as a co-factor. Consequently, photon output is thought to be positively correlated with tumor mass. As expected, strong correlations were observed between BLI and tumor burden in all models. Additionally, no interaction was observed between types of tumor model and R², suggesting that BLI remains a valid tool for assessing tumor burden of xenografts in mouse models, regardless of the site of inoculation. However, a high degree of variabilities in correlation values was also observed in our analysis. This may be explained by the limitations of BLI techniques. Since luciferase requires ATP and oxygen for light output, it is not surprising that the most reported factor that led to a poor correlation was the presence of necrosis or hypoxia in the tumors assessed. In the model developed by Godechal *et al.*

to characterize melanoma, the authors suggested that the poor correlation between BLI and tumor weight was due to lack of oxygen and poor perfusion. As a result, limited substrate as well as cofactor (O₂) led to underestimation of tumor mass by BLI (15). Moreover, in another s.c. xenograft model developed for detection of breast cancer, the authors also discussed the impact of hypoxia and necrosis on the extent of correlation between BLI and tumor burden (10). In their study, it was found that a good correlation existed between BLI and tumor volume in tumors with a diameter of less than 1.2 cm (10). In contrast, as tumors got larger, the correlation became inferior (data not shown) due to excessive necrosis. A similar result was reported in another study using a glioma model (16). Furthermore, in the s.c. colon cancer model developed by Hadaschik *et al.*, attenuation of light signal was observed at advanced

disease stages. It was suggested that an increased necrosis may be responsible for the discrepancy between tumor volume and *in vivo* BLI signal (17). A decrease in bioluminescent signal in areas of necrosis was further confirmed histologically in two separate studies (18,19).

Another major limitation of BLI is signal quenching. It is well known that light generated from luciferase is prone to tissue attenuation (20). In the i.p. gastric cancer model by Stollfuss and colleagues, the poor correlation between tumor volume and BLI was attributed to light scattering and absorption from tissue and organs (21). Specifically, a high detection rate of metastatic lesions was observed for those that invaded the peritoneum, whereas none of the lesions on the diaphragm, and only 1/13 of the lesions on the liver were detected (21). Another example of light quenching was demonstrated in a syngeneic, orthotopic, murine bladder model where bioluminescent signal was reduced in the hemorrhagic tumor area (22). Hemoglobin in red blood cells can decrease light penetration (23). In addition, surrounding tissue may also be affected by blood coming from the site of hemorrhaging, thereby leading to further reduction of photon emission.

Besides tissue attenuation, accumulation of ascites also has the potential to prevent light penetration. In this review, we identified two studies using ascetic models that reported correlations between BLI signaling and tumor burden. Interestingly, an excellent R^2 of 0.8 (24) and 0.98 (25) was seen in both studies. In contrast, in an i.p. disseminated xenograft model of ovarian cancer recently developed by our group, we observed a reduction in bioluminescence after widespread ascites formation, which resulted in an inferior correlation (26). This is consistent with a previous study of an intrahepatic model developed by Sarraf-Yazdi *et al.* in which the correlation improved after paracentesis (27). The study by Sarraf-Yazdi *et al.* was not included in this review as a non-linear correlation was performed. The discrepancy observed between our group and the identified literature in this review may be explained by the difference in the volume of ascites fluid and the technique used to measure tumor burden. While our study was associated with an accumulation of more than 4 mL of ascites within the peritoneal cavity of mice, the study by Lan *et al.* (24) reported volumes of less than 0.4 mL in their model. These amounts of fluid likely have minimal impact on the BLI output. Additionally, in models by both Sarraf-Yazdi *et al.*

(27) and our group, tumor burden was measured by weight. In contrast, in the study by Edinger *et al.*, FACS was used to measure tumor burden in the liver and spleen (25). This suggests that in the presence of ascites fluid, tumor burden may be better measured by a combination of different techniques.

Discrepancies between BLI signal and tumor burden are often associated with advanced disease stages, which typically involve large tumors and sometimes the onset of ascites. Therefore, we sought to determine whether there is an interaction between tumor progression and the validity of BLI. However, no relationship was observed ($p=0.1679$). The inconclusive result was likely due to the heterogeneous nature of the data collected in this study. For example, it is known that different cancer cell lines exhibit distinct doubling times, and the data collected for this analysis consist of models developed from a diverse range of human or murine cancer cell lines inoculated into various strains of mice. As such, one can expect that advanced stages of tumor progression for one model may be at an optimal time for imaging in another model. It is plausible that if a large enough dataset of correlations were to be collected at various time points from the same model, a discrete interaction may be observed.

Next, we attempted to investigate the effect of route of substrate delivery on the correlation between BLI and tumor burden. Unfortunately, a comparison could not be made due to the fact that large majority of the models administered the luciferase substrate only through i.p. injection. However, route of substrate administration remains a factor to be considered when utilizing BLI as it has been shown that administration of intravenous luciferin resulted in differential tissue uptake and time to the peak signal than intraperitoneal administration (11).

One important observation demonstrated by this review is that xenograft models developed from clonally selected cell populations demonstrate a superior correlation between BLI and tumor burden. When creating a bioluminescent xenograft model, a plasmid typically containing genes for both luciferase and antibiotic resistance is introduced to cancer cells by transfection or transduction (28). While addition of antibiotic allows for selection of successfully transfected or transduced cells, there is no control of the copy number of the plasmid that was introduced to the cells. This results in a heterogeneous cell population with differential luciferase expression. Since light intensity is proportional to the copy number of luciferases (29),

using a mixed cell population can possibly lead to inconsistent photon emission throughout a tumor nodule, thereby impacting the correlation. In addition, loss of copy number of the luciferase gene has been demonstrated in large s.c. tumors leading to a poor correlation. Therefore, selection of a single cell clone with the highest luciferase expression is recommended. However, one major limitation associated with clonally selected cell population is the loss of heterogeneity, which can impact the clinical relevance of the tumor model.

Imaging technology plays a crucial role in the detection of cancer. Beyond the traditional methods of tumor measurement by caliper and weight, imaging techniques such as Computed Tomography (CT), Magnetic Resonance Imaging (MRI), Positron Emission Tomography (PET) and ultrasound have also been used to assess tumor burden. Interestingly, a negative relationship was found between BLI and tumor burden measured using non-BLI imaging-based techniques, likely due to wide range of correlation values observed. A possible explanation for the discrepancies observed in this cohort could be the technical expertise required to operate these systems. While studies using ultrasound and PET generally resulted in a strong correlation (30–32), models with CT and MRI can result in a inferior correlation. In a model of breast cancer, the authors commented that the inferior correlation between BLI and CT-based assessment of tumor burden was likely due to poor animal positioning and tissue attenuation (33). Furthermore, while CT imaging provides high resolution imaging of bony structures, its soft tissue visualization is limited (1). As such, a combination of technical limitations and human error likely contributed to the inability of CT to detect tumors in this case. In another study assessing tumor burden using MRI, the low correlation with BLI was attributed to motion artefacts from animal respiration (34). However, when respiration synchronized images were taken, the correlation was improved. Therefore, although technical error is associated with optical imaging, when properly controlled, a good correlation between BLI and tumor burden can be achieved (35–38).

Despite being regarded as a highly sensitive and reliable method for evaluating tumor burden *in vivo*, the accuracy of BLI model may still be impacted by various factors. However, it is surprising that validation of BLI models before subsequent experimentations is rarely performed. Of the 1870 publications that underwent full text screening, 76%

(1422/1870) did not report a correlation between BLI and tumor burden, and only 6% (116/1870) validated the model. This observation is alarming as an invalid model can lead to incorrect conclusions. Although there are limitations that are intrinsic to some tumor models (hypoxia, tissue attenuation) and difficult to control, parameter such as imaging time is surprisingly overlooked by researchers. It has been shown in several studies that the peak bioluminescent signal is reached approximately 10 minutes after an i.p. injection of d-luciferin (12,39,40). However, almost half of the eligible publications (54/116) did not report the timing of BLI relative to the administration of d-luciferin, and of those that did report, only 32 groups had taken the image at the peak bioluminescent signal, as reported previously (*i.e.* at 10 minutes after i.p. injection). Additionally, the work by Inoue *et al.* suggested that the timing of peak signal shifts depends on the number of days post-inoculation. Therefore, acquisition of BLI images at a predetermined time point may become inaccurate as the tumor progresses and therefore obtaining successive images may improve tumor monitoring by capturing the peak bioluminescent signal. Indeed, our regression analysis demonstrated a significant positive relationship between R^2 values and sequential imaging ($p < 0.05$). As such, it is recommended that sequential images be acquired to avoid underestimation of tumor burden.

CONCLUSION

Collectively, we have shown that BLI remains a valid tool for preclinical assessment of tumor growth and drug response. Since many factors can influence BLI, conflicting results on its correlation to tumor burden have been reported as shown by the high disparity observed across the analysis. Therefore, no single entity may be identified as a general limitation of the BLI technique. As such, we propose the following considerations when utilizing BLI in small animal imaging: 1) derive xenografts using single-cell populations with the highest luciferase expression using the limiting dilution method; 2) use appropriate non-BLI assessment methods to confirm tumor burden depending on the model of choice; 3) acquire sequential images to capture the peak bioluminescent signal; 4) BLI may become less reliable at advanced disease stages, thus traditional efficacy assessments such as median survival should be employed to complement the overall analysis. In

light of this, we hope to bring consensus between researchers and to refine the approach to BLI-based assessment of tumor burden in preclinical xenograft cancer models.

CONFLICT OF INTEREST

Authors declare no conflict of interest.

ABBREVIATIONS

s.c. Subcutaneous
i.p. Intraperitoneal
o.t. Orthotopic
i.v. Intravenous

ACKNOWLEDGEMENT

The authors thank Drs. Alex Kiss and Xingshan Cao for their expertise on statistical analysis. Y.T. Shen was funded by a scholarship from the Leslie Dan Faculty of Pharmacy Dean's Funding. C.A. and M.P.-M. acknowledge the funding support from the Ovarian Cancer Research Program, Congressionally Directed Medical Research Program, Department of Defense (Award number W81XWH-16-1-0388).

REFERENCES

- WangY, TsengJ-C, SunY, BeckAH, KungAL. Noninvasive imaging of tumor burden and molecular pathways in mouse models of cancer. *Cold Spring Harb Protoc.* 2015;2015(2):135–44.
- KooV, HamiltonPW, WilliamsonK. Non-invasive in vivo imaging in small animal. 2006;28:127–39.
- PaleyMA, PrescherJA. Bioluminescence: A versatile technique for imaging cellular and molecular features. *Medchemcomm.* 2014;5(3):255–67.
- JenkinsDE, OeiY, HornigYS, YuS-F, DusichJ, PurchioT, et al. Bioluminescent imaging (BLI) to improve and refine traditional murine models of tumor growth and metastasis. *Clin Exp Metastasis.* 2003;20(8):733–44.
- KlerkCPW, OvermeerRM, NiersTMH, VersteegHH, RichelDJ, BuckleT, et al. Validity of bioluminescence measurements for noninvasive in vivo imaging of tumor load in small animals. *Biotechniques.* 2007;43(1 Suppl):7–13.
- DothagerRS, FlentieK, MossB, PanMH, KesarwalaA, Piwnica-WormsD. Advances in bioluminescence imaging of live animal models. *Curr Opin Biotechnol.* 2009;20(1):45–53.
- LyonsSK. Advances in imaging mouse tumour models in vivo. *J Pathol.* 2005;205(2):194–205.
- BadrCE. *Bioluminescent Imaging: Basics and Practical Limitations.* 2014;1098(January).
- TuliR, SurmakA, ReyesJ, Hacker-PrietzA, ArmourM, LeubnerA, et al. Development of a novel preclinical pancreatic cancer research model: bioluminescence image-guided focal irradiation and tumor monitoring of orthotopic xenografts. *Transl Oncol.* 2012;5(2):77–84.
- ShanL, WangS, KorotcovA, SridharR, WangPC. Bioluminescent animal models of human breast cancer for tumor biomass evaluation and metastasis detection. *Ethn Dis.* 2008;18(2 Suppl 2):S2-S65-9.
- BergerF, PaulmuruganR, BhaumikS, GambhirSS. Uptake kinetics and biodistribution of ¹⁴C-d-luciferin—a radiolabeled substrate for the firefly luciferase catalyzed bioluminescence reaction: impact on bioluminescence based reporter gene imaging. *Eur J Nucl Med Mol Imaging.* 2008 Dec 26;35(12):2275–85.
- InoueY, KiryuS, IzawaK, WatanabeM, TojoA, OhtomoK. Comparison of subcutaneous and intraperitoneal injection of D-luciferin for in vivo bioluminescence imaging. *Eur J Nucl Med Mol Imaging.* 2009;36(5):771–9.
- BaertT, VerschuereT, VanHoylandtA, GijsbersR, VergoteI, CoosemansA. The dark side of ID8-Luc2: Pitfalls for luciferase tagged murine models for ovarian cancer. *J Immunother Cancer.* 2015;3(1):57.
- KalraJ, AnanthaM, WarburtonC, WaterhouseD, YanH, YangY-J, et al. Validating the use of a luciferase labeled breast cancer cell line, MDA435LCC6, as a means to monitor tumor progression and to assess the therapeutic activity of an established anticancer drug, docetaxel (Dt) alone or in combination with the ILK inhibitor. *Cancer Biol Ther.* 2011;11(9):826–38.
- GodechalQ, DefresneF, DanhierP, LevequeP, PorporatoPE, SonveauxP, et al. Assessment of melanoma extent and melanoma metastases invasion using electron paramagnetic resonance and bioluminescence imaging. *Contrast Media Mol Imaging.* 2011;6(4):282–8.
- JangSJ, KangJH, KimKII, LeeTS, LeeYJ, LeeKC, et al. Application of bioluminescence imaging to therapeutic intervention of herpes simplex virus type I – Thymidine kinase/ganciclovir in glioma. *Cancer Lett.* 2010 Nov 1;297(1):84–90.
- InoueY, ShengF, KiryuS, WatanabeM, RatanakanitH, IzawaK, et al. Gaussia luciferase for bioluminescence tumor monitoring in comparison with firefly luciferase. *Mol Imaging.* 2011;10(5):377–85.
- SölingA, TheißC, JungmichelS, RainovNG. A dual function fusion protein of Herpes simplex

- virus type 1 thymidine kinase and firefly luciferase for noninvasive in vivo imaging of gene therapy in malignant glioma. *Genet Vaccines Ther.* 2004 Aug 4;2(1):7.
19. HundtW, SteinbachS, O'Connell-RodwellCE, MayerD, BednarskiMD, GuccioneS. Tumor tissue characterization evaluating the luciferase activity under the control of a hsp70 promoter and MR imaging in three tumor cell lines. *Eur J Radiol.* 2009;70(2):369–77.
 20. VirostkoJ, ChenZ, FowlerM, PoffenbergerG, PowersAC, Duco JansenE. Factors influencing quantification of in vivo bioluminescence imaging: Application to assessment of pancreatic islet transplants. *Mol Imaging.* 2004 Oct;3(4):333–42.
 21. StollfussJ, LandvogtN, AbensteinM, ZieglerS, SchwaigerM, Senekowitsch-SchmidtkeR, et al. Non-invasive imaging of implanted peritoneal carcinomatosis in mice using PET and bioluminescence imaging. *EJNMMI Res.* 2015;5(1):125.
 22. JurczokA, FornaraP, SölingA. Bioluminescence imaging to monitor bladder cancer cell adhesion in vivo: a new approach to optimize a syngeneic, orthotopic, murine bladder cancer model. *BJU Int.* 2007 Sep 20;0(0):070921231855001-???
 23. ColinM, MoritzS, SchneiderH, CapeauJ, CoutelleC, Brahimi-HornMC. Haemoglobin interferes with the ex vivo luciferase luminescence assay: Consequence for detection of luciferase reporter gene expression in vivo. *Gene Ther.* 2000 Aug;7(15):1333–6.
 24. LanKL, Ou-YangF, YenSH, ShihHL, LanKH. Cationic liposome coupled endostatin gene for treatment of peritoneal colon cancer. *Clin Exp Metastasis.* 2010;27(5):307–18.
 25. EdingerM, CaoY-A, VermerisMR, BachmannMH, ContagCH, NegrinRS. Revealing lymphoma growth and the efficacy of immune cell therapies using in vivo bioluminescence imaging. *Blood.* 2003 Jan 15;101(2):640–8.
 26. ShenYT, WangL, EvansJC, AllenC, Piquette-MillerM. Development of a Bioluminescent BRCA1-Deficient Xenograft Model of Disseminated, High-Grade Serous Ovarian Cancer. *Int J Mol Sci.* 2019 May 21;20(10):2498.
 27. Sarraf-YazdiS, MiJ, DewhirstMW, ClaryBM. Use of in Vivo bioluminescence imaging to predict hepatic tumor burden in mice. *J Surg Res.* 2004;120(2):249–55.
 28. KeyaertsM, CaveliersV, LahoutteT. Bioluminescence imaging: looking beyond the light. *Trends Mol Med.* 2012;18(3):164–72.
 29. FeysL, DescampsB, VanhoveC, VermeulenS, VandesompeleJO, VanderheydenK, et al. Quantitative and Functional Requirements for Bioluminescent Cancer Models. *In Vivo.* 30(1):1–11.
 30. LardizabalJ, DingJ, DelwarZ, RenniePS, JiaW. A TRAMP-derived orthotopic prostate syngeneic (TOPS) cancer model for investigating anti-tumor treatments. *Prostate.* 2018;78(6):457–68.
 31. TeitzT, StankeJJ, FedericoS, BradleyCL, BrennanR, ZhangJ, et al. Preclinical models for Neuroblastoma: Establishing a baseline for treatment. *PLoS One.* 2011;6(4).
 32. AdisheshaiahPP, PatelNL, IlevaLV, KalenJD, HainesDC, McNeilSE. Longitudinal imaging of cancer cell metastases in two preclinical models: a correlation of noninvasive imaging to histopathology. *Int J Mol Imaging.* 2014;2014:102702.
 33. FrickeIB, DeSouzaR, Costa AyubL, FranciaG, KerbelR, JaffrayDA, et al. Spatiotemporal assessment of spontaneous metastasis formation using multimodal in vivo imaging in HER2+ and triple negative metastatic breast cancer xenograft models in mice. *PLoS One.* 2018;13(5):e0196892.
 34. BianchiA, DufortS, FortinP-Y, LuxF, RaffardG, TassaliN, et al. In vivo MRI for effective non-invasive detection and follow-up of an orthotopic mouse model of lung cancer. *NMR Biomed.* 2014;27(8):971–9.
 35. ShiJ, UdayakumarTS, WangZ, DoganN, PollackA, YangY. Optical molecular imaging-guided radiation therapy part 1: Integrated x-ray and bioluminescence tomography. *Med Phys.* 2017;44(9):4786–94.
 36. TuliR, SurmakA, ReyesJ, Hacker-PrietzA, ArmourM, LeubnerA, et al. Development of a Novel Preclinical Pancreatic Cancer Research Model: Bioluminescence Image- Guided Focal Irradiation and Tumor Monitoring of Orthotopic Xenografts. *Transl Oncol.* 2012;5(2):77–84.
 37. RagelBT, ElamIL, GillespieDL, FlynnJR, KellyD a, MabeyD, et al. A novel model of intracranial meningioma in mice using luciferase-expressing meningioma cells. Laboratory investigation. *J Neurosurg.* 2008;108(2):304–10.
 38. HsuAR, CaiW, VeeravaguA, MohamedaliKA, ChenK, KimS, et al. Multimodality molecular imaging of glioblastoma growth inhibition with vasculature-targeting fusion toxin VEGF121/rGel. *J Nucl Med.* 2007;48(3):445–54.
 39. ParooZ, BollingerRA, BraaschDA, RicherE, CoreyDR, AntichPP, et al. Validating Bioluminescence Imaging as a High-Throughput, Quantitative Modality for Assessing Tumor Burden. *Mol Imaging.* 2004 Apr;3(2):153535002004031.
 40. InoueY, KiryuS, WatanabeM, TojoA, OhtomoK. Timing of imaging after D-luciferin injection affects the longitudinal assessment of tumor

- growth using in vivo bioluminescence imaging. *Int J Biomed Imaging*. 2010;2010.
41. Notting IC, Buijs JT, Quel, Mintardjo RE, van der Horst G, Karperien M, et al. Whole-Body Bioluminescent Imaging of Human Uveal Melanoma in a New Mouse Model of Local Tumor Growth and Metastasis. *Investig Ophthalmology Vis Sci*. 2005;46(5):1581.
 42. Goldman SJ, Chen E, Taylor R, Zhang S, Petrosky W, Reiss M, et al. Use of the ODD-luciferase transgene for the non-invasive imaging of spontaneous tumors in mice. *PLoS One*. 2011;6(3).
 43. Hiraoka K, Kimura T, Logg CR, Tai CK, Haga K, Lawson GW, et al. Therapeutic efficacy of replication-competent retrovirus vector-mediated suicide gene therapy in a multifocal colorectal cancer metastasis model. *Cancer Res*. 2007;67(11):5345–53.
 44. Nyati MK, Symon Z, Kievit E, Dornfeld KJ, Rynkiewicz SD, Ross BD, et al. The potential of 5-fluorocytosine/cytosine deaminase enzyme prodrug gene therapy in an intrahepatic colon cancer model. *Gene Ther*. 2002;9(13):844–9.
 45. Noh K, Kim K-O, Patel NR, Staples JR, Minematsu H, Nair K, et al. Targeting inflammatory kinase as an adjuvant treatment for osteosarcomas. *J Bone Joint Surg Am*. 2011;93(8):723–32.
 46. Bianchi A, Dufort S, Lux F, Fortin P-Y, Tassali N, Tillement O, et al. Targeting and in vivo imaging of non-small-cell lung cancer using nebulized multimodal contrast agents. *Proc Natl Acad Sci U S A*. 2014;111(25):9247–52.
 47. Mayr U, VonWerder A, Seidler B, Reindl W, Bajbouj M, Schmid RM, et al. RCAS-mediated retroviral gene delivery: a versatile tool for the study of gene function in a mouse model of pancreatic cancer. *Hum Gene Ther*. 2008;19(9):896–906.
 48. Casarez EV, Dunlap-Brown ME, Conaway MR, Amorino GP. Radiosensitization and modulation of p44/42 mitogen-activated protein kinase by 2-methoxyestradiol in prostate cancer models. *Cancer Res*. 2007;67(17):8316–24.
 49. Fushiki H, Kanoh-Azuma T, Katoh M, Kawabata K, Jiang J, Tsuchiya N, et al. Quantification of mouse pulmonary cancer models by microcomputed tomography imaging. *Cancer Sci*. 2009;100(8):1544–9.
 50. Fleshker S, Preisd D, Kalchenko V, Scherz A, Salomon Y. Prompt assessment of WST11-VTP outcome using luciferase transfected tumors enables second treatment and increase in overall therapeutic rate. *Photochem Photobiol*. 2008;84(5):1231–7.
 51. Wang Q, Luan W, Goz V, Burakoff SJ, Hiottis SP. Non-invasive in vivo imaging for liver tumour progression using an orthotopic hepatocellular carcinoma model in immunocompetent mice. *Liver Int*. 2011;31(8):1200–8.
 52. Riedel SS, Mottok A, Brede C, Bäuerlein CA, Jordán Garrote AL, Ritz M, et al. Non-Invasive Imaging Provides Spatiotemporal Information on Disease Progression and Response to Therapy in a Murine Model of Multiple Myeloma. *PLoS One*. 2012;7(12).
 53. Sonabend AM, Yun J, Lei L, Leung R, Soderquist C, Crisman C, et al. Murine cell line model of proneural glioma for evaluation of anti-tumor therapies. *J Neurooncol*. 2013;112(3):375–82.
 54. Katsuta E, Rashid OM, Takabe K. Murine breast cancer mastectomy model that predicts patient outcomes for drug development. *J Surg Res*. 2017;219:310–8.
 55. Pool SE, ten Hagen TLM, Koelewijn S, de Jong M, Koning GA. Multimodality imaging of somatostatin receptor-positive tumors with nuclear and bioluminescence imaging. *Mol Imaging*. 2012;11(1):27–32.
 56. Mandl SJ, Mari C, Edinger M, Negrin RS, Tait JF, Contag CH, et al. Multi-modality imaging identifies key times for annexin V imaging as an early predictor of therapeutic outcome. *Mol Imaging*. 2004;3(1):1–8.
 57. Wu T, Heuillard E, Lindner V, Bou About G, Ignat M, Dillenseger J-P, et al. Multimodal imaging of a humanized orthotopic model of hepatocellular carcinoma in immunodeficient mice. *Sci Rep*. 2016;6:35230.
 58. Li L, Mori S, Sakamoto M, Takahashi S, Kodama T. Mouse model of lymph node metastasis via afferent lymphatic vessels for development of imaging modalities. *PLoS One*. 2013;8(2):e55797.
 59. Iochmann S, Lerondel S, Blechet C, Lavergne M, Pesnel S, Sobilo J, et al. Monitoring of tumour progression using bioluminescence imaging and computed tomography scanning in a nude mouse orthotopic model of human small cell lung cancer. *Lung Cancer*. 2012;77(1):70–6.
 60. Hundt W, Steinbach S, O'Connell-Rodwell CE, Mayer D, Burbelko M, Guccione S. In vivo monitoring of antiangiogenic therapy by magnetic resonance and bioluminescence imaging in an M21 tumor model through activation of an hsp70 promoter-luciferase reporter construct. *Contrast Media Mol Imaging*. 2012;7(5):450–9.
 61. Otto-Duessel M, Khankaldyyan V, Gonzalez-Gomez I, Jensen MC, Laug WE, Rosol M. In vivo testing of Renilla luciferase substrate analogs in an orthotopic murine model of human glioblastoma. *Mol Imaging*. 2006;5(2):57–64.
 62. Hsu AR, Hou LC, Veeravagu A, Greve JM, Vogel H, Tse V, et al. In vivo near-infrared fluorescence

- imaging of integrin $\alpha\beta3$ in an orthotopic glioblastoma model. *Mol Imaging Biol.* 2006;8(6):315–23.
63. KirschnerS, FelixMC, HartmannL, BierbaumM, MarosME, KerlHU, et al. In vivo micro-CT imaging of untreated and irradiated orthotopic glioblastoma xenografts in mice: capabilities, limitations and a comparison with bioluminescence imaging. *J Neurooncol.* 2015;122(2):245–54.
64. ScatenaCD, HepnerMA, OeiYA, DusichJM, YuS-F, PurchioT, et al. Imaging of bioluminescent LNCaP-luc-M6 tumors: A new animal model for the study of metastatic human prostate cancer. *Prostate.* 2004;59(3):292–303.
65. SunA, HouL, PrugpichailersT, DunkelJ, KalaniMA, ChenX, et al. Firefly luciferase-based dynamic bioluminescence imaging: a noninvasive technique to assess tumor angiogenesis. *Neurosurgery.* 2010;66(4):751–7.
66. MorinaA, RuggieroC, RobidelE, Doghman-BouguerraM, DasAT, CastellanoR, et al. Establishment of a mouse xenograft model of metastatic adrenocortical carcinoma. *Oncotarget.* 2017;8(31):51050–7.
67. BaumannBC, KaoGD, MahmudA, HaradaT, SwiftJ, ChapmanC, et al. Enhancing the efficacy of drug-loaded nanocarriers against brain tumors by targeted radiation therapy. *Oncotarget.* 2013;4(1):64–79.
68. PuauxA-L, OngLC, JinY, TehI, HongM, ChowPKH, et al. A comparison of imaging techniques to monitor tumor growth and cancer progression in living animals. *Int J Mol Imaging.* 2011;2011:321538.
69. ParkinsKM, HamiltonAM, MakelaAV, ChenY, FosterPJ, RonaldJA. A multimodality imaging model to track viable breast cancer cells from single arrest to metastasis in the mouse brain. *Sci Rep.* 2016;6:35889.
70. HuangJ, LiYM, ChengQ, ValleraDA, HallWA. A novel brain metastasis xenograft model for convection-enhanced delivery of targeted toxins via a micro-osmotic pump system enabled for real-time bioluminescence imaging. *Mol Med Rep.* 2015;12(4):5163–8.
71. LupoldSE, JohnsonT, ChowdhuryWH, RodriguezR. A real time Metridia luciferase based non-invasive reporter assay of mammalian cell viability and cytotoxicity via the beta-actin promoter and enhancer. *PLoS One.* 2012;7(5):e36535.
72. KimuraJ, OnoHA, KosakaT, NagashimaY, HiraiS, OhnoS, et al. Conditionally replicative adenoviral vectors for imaging the effect of chemotherapy on pancreatic cancer cells. *Cancer Sci.* 2013;104(8):1083–90.
73. DevaudC, RousseauB, NetzerS, PitardV, ParoissinC, KhairallahC, et al. Anti-metastatic potential of human Vdelta1(+) gammadelta T cells in an orthotopic mouse xenograft model of colon carcinoma. *Cancer Immunol Immunother.* 2013;62(7):1199–210.
74. XinJ, ZhanY, LiuM, HuH, XiaL, NieY, et al. ApoG2 induces ER stress-dependent apoptosis in gastric cancer cells in vitro and its real-time evaluation by bioluminescence imaging in vivo. *Cancer Lett.* 2013;336(2):260–9.
75. AuJT, GonzalezL, ChenC-H, SerganovaI, FongY. Bioluminescence imaging serves as a dynamic marker for guiding and assessing thermal treatment of cancer in a preclinical model. *Ann Surg Oncol.* 2012;19(9):3116–22.
76. YeramianA, GarciaV, BergadaL, DomingoM, SantacanaM, VallsJ, et al. Bioluminescence Imaging to Monitor the Effects of the Hsp90 Inhibitor NVP-AUY922 on NF-kappaB Pathway in Endometrial Cancer. *Mol Imaging Biol.* 2016;18(4):545–56.
77. WangY, SunZ, PengJ, ZhanL. Bioluminescent imaging of hepatocellular carcinoma in live mice. *Biotechnol Lett.* 2007;29(11):1665–70.
78. ZhongR, PytyniaM, PelizzariC, SpiottoM. Bioluminescent imaging of HPV-positive oral tumor growth and its response to image-guided radiotherapy. *Cancer Res.* 2014;74(7):2073–81.
79. GhoshM, GambhirSS, DeA, NowelsK, GorisM, WapnirI. Bioluminescent monitoring of NIS-mediated ^{131}I ablative effects in MCF-7 xenografts. *Mol Imaging.* 2006;5(2):76–84.
80. GiubellinoA, WoldemichaelGM, SourbierC, LizakMJ, PowersJF, TischlerAS, et al. Characterization of two mouse models of metastatic pheochromocytoma using bioluminescence imaging. *Cancer Lett.* 2012;316(1):46–52.
81. TangF-Y, PaiM-H, KuoY-H, WangX-D. Concomitant consumption of lycopene and fish oil inhibits tumor growth and progression in a mouse xenograft model of colon cancer. *Mol Nutr Food Res.* 2012;56(10):1520–31.
82. CaceresG, ZankinaR, ZhuX, JiaoJ, WongH, AllerA, et al. Determination of chemotherapeutic activity in vivo by luminescent imaging of luciferase-transfected human tumors. *Anticancer Drugs.* 2003;14(7):569–74.
83. ZhouH, Luby-PhelpsK, MickeyBE, HabibAA, MasonRP, ZhaoD. Dynamic Near-Infrared Optical Imaging of 2-Deoxyglucose Uptake by Intracranial Glioma of Athymic Mice. *PLoS One.* 2009;4(11):1–9.
84. MaX, LiuZ, YangX, GaoQ, ZhuS, QinC, et al. Dual-modality monitoring of tumor response to cyclophosphamide therapy in mice with

- bioluminescence imaging and small-animal positron emission tomography. *Mol Imaging*. 2011;10(4):278–83.
85. ButterworthKT, RedmondKM, McMahonSJ, ColeAJ, JainS, McCarthyHO, et al. Conventional in vivo irradiation procedures are insufficient to accurately determine tumor responses to non-uniform radiation fields. *Int J Radiat Biol*. 2015;91(3):257–61.
 86. YahyanejadS, GrantonPV, LieuwesNG, GilmourL, DuboisL, TheysJ, et al. Complementary use of bioluminescence imaging and contrast-enhanced micro-computed tomography in an orthotopic brain tumor model. *Mol Imaging*. 2014;13.
 87. PoeschingerT, RennerA, WeberT, ScheuerW. Bioluminescence imaging correlates with tumor serum marker, organ weights, histology, and Human DNA levels during treatment of orthotopic tumor xenografts with antibodies. *Mol Imaging Biol*. 2013;15(1):28–39.
 88. RonaldJA, D’SouzaAL, ChuangH-Y, GambhirSS. Artificial MicroRNAs as Novel Secreted Reporters for Cell Monitoring in Living Subjects. *PLoS One*. 2016;11(7):e0159369.
 89. R.A.L, C.N.F, J.Y, J.Y.L, M.A.W, Q.T.N, et al. An optimized triple modality reporter for quantitative in vivo tumor imaging and therapy evaluation. *PLoS One*. 2014;9(5):e97415.
 90. HadaschikBA, BlackPC, SeaJC, MetwalliAR, FazliL, DinneyCP, et al. A validated mouse model for orthotopic bladder cancer using transurethral tumour inoculation and bioluminescence imaging. *BJU Int*. 2007;100(6):1377–84.
 91. TakahashiR, YokoboriT, OsoneK, TatsukiH, TakadaT, SutoT, et al. Establishment of a novel method to evaluate peritoneal microdissemination and therapeutic effect using luciferase assay. *Cancer Sci*. 2016;107(3):341–6.
 92. LiuIH, ChangCH, HoCL, ChiuSP, LeeWC, ChangTJ, et al. Multimodality imaging and preclinical evaluation of ¹⁷⁷Lu-AMBA for human prostate tumours in a murine model. *Anticancer Res*. 2010;30(10):4039–48.
 93. RamasawmyR, JohnsonSP, RobertsTA, StuckeyDJ, DavidAL, PedleyRB, et al. Monitoring the growth of an orthotopic tumour xenograft model: Multi-Modal imaging assessment with benchtop MRI (1T), high-Field MRI (9.4T), ultrasound and bioluminescence. *PLoS One*. 2016;11(5):1–16.
 94. JeonYH, ChoiY, KimHJ, KangJH, KimCW, JeongJM, et al. In vivo bioluminescence visualization of antitumor effects by human MUC1 vaccination. *Mol Imaging*. 2007;6(5):297–303.
 95. ZhengJ, XuL, ZhouH, ZhangW, ChenZ. Quantitative analysis of cell tracing by in vivo imaging system. *J Huazhong Univ Sci Technolog Med Sci*. 2010;30(4):541–5.
 96. ShinJH, ChungJ-K, KangJH, LeeYJ, KimKII, SoY, et al. Noninvasive imaging for monitoring of viable cancer cells using a dual-imaging reporter gene. *J Nucl Med*. 2004;45(12):2109–15.
 97. MaesW, DerooseC, ReumersV, KrylyshkinaO, GijssbersR, BaekelandtV, et al. In vivo bioluminescence imaging in an experimental mouse model for dendritic cell based immunotherapy against malignant glioma. *J Neurooncol*. 2009;91(2):127–39.
 98. HuH, LiuJ, YaoL, YinJ, SuN, LiuX, et al. Real-time bioluminescence and tomographic imaging of gastric cancer in a novel orthotopic mouse model. *Oncol Rep*. 2012;27(6):1937–43.
 99. ChungE, YamashitaH, AuP, TannousBA, FukumuraD, JainRK. Secreted Gaussia luciferase as a biomarker for monitoring tumor progression and treatment response of systemic metastases. *PLoS One*. 2009;4(12):e8316.
 100. ParooZ, BollingerRA, BraaschDA, RicherE, CoreyDR, AntichPP, et al. Validating bioluminescence imaging as a high-throughput, quantitative modality for assessing tumor burden. *Mol Imaging*. 2004;3(2):117–24.
 101. CraftN, BruhnKW, NguyenBD, PrinsR, LiauLM, CollissonEA, et al. Bioluminescent Imaging of Melanoma in Live Mice. *J Invest Dermatol*. 2005 Jul;125(1):159–65.
 102. ZhangC, YanZ, ArangoME, PainterCL, AnderesK. Advancing bioluminescence imaging technology for the evaluation of anticancer agents in the MDA-MB-435-HAL-Luc mammary fat pad and subrenal capsule tumor models. *Clin Cancer Res*. 2009;15(1):238–46.
 103. YanagiharaK, TakigahiraM, TakeshitaF, KomatsuT, NishioK, HasegawaF, et al. A Photon Counting Technique for Quantitatively Evaluating Progression of Peritoneal Tumor Dissemination. *Cancer Res*. 2006 Aug 1;66(15):7532–9.
 104. ColomboP-E, BousttaM, PoujoIS, JarlierM, BressolleF, TeulonI, et al. Intraperitoneal administration of novel doxorubicin loaded polymeric delivery systems against peritoneal carcinomatosis: Experimental study in a murine model of ovarian cancer. *Gynecol Oncol*. 2011 Sep;122(3):632–40.
 105. JägerW, MoskalevI, JanssenC, HayashiT, AwreyS, GustKM, et al. Ultrasound-Guided Intramural Inoculation of Orthotopic Bladder Cancer Xenografts: A Novel High-Precision Approach. *PLoS One*. 2013;8(3):1–11.
 106. VooijsM, JonkersJ, LyonsS, BernsA. Noninvasive imaging of spontaneous

- retinoblastoma pathway-dependent tumors in mice. *Cancer Res.* 2002 Mar 15;62(6):1862–7.
107. AlhasanMK, LiuL, LewisMA, MagnussonJ, MasonRP. Comparison of Optical and Power Doppler Ultrasound Imaging for Non-Invasive Evaluation of Arsenic Trioxide as a Vascular Disrupting Agent in Tumors. KanoMR, editor. *PLoS One.* 2012 Sep 28;7(9):e46106.
 108. ShibataMA, ShibataE, MorimotoJ, EidNAS, TanakaY, WatanabeM, et al. An immunocompetent murine model of metastatic mammary cancer accessible to bioluminescence imaging. *Anticancer Res.* 2009;29(11):4389–95.
 109. KogureT, KinghornAD, YanI, BolonB, LucasDM, GreverMR, et al. Therapeutic Potential of the Translation Inhibitor Silvestrol in Hepatocellular Cancer. VinciguerraM, editor. *PLoS One.* 2013 Sep 26;8(9):e76136.
 110. JiX, ChengL, WeiF, LiH, WangM, TianY, et al. Noninvasive visualization of retinoblastoma growth and metastasis via bioluminescence imaging. *Investig Ophthalmol Vis Sci.* 2009;50(12):5544–51.
 111. ComstockKE, HallCL, DaignaultS, MandlebaumSA, YuC, KellerET. A bioluminescent orthotopic mouse model of human osteosarcoma that allows sensitive and rapid evaluation of new therapeutic agents *In vivo.* *In Vivo.* 23(5):661–8.
 112. FengM, ZhangJ, AnverM, HassanR, HoM. *In vivo* imaging of human malignant mesothelioma grown orthotopically in the peritoneal cavity of nude mice. *J Cancer.* 2011 Mar 1;2:123–31.
 113. LanKL, YenSH, LiuRS, ShihHL, TsengFW, LanKH. Mutant Bik gene transferred by cationic liposome inhibits peritoneal disseminated murine colon cancer. *Clin Exp Metastasis.* 2007;24(6):461–70.
 114. KimS-J, SeoHK, SeoH-H, LeeS-J, KwonJK, LeeT-J, et al. Establishment of an orthotopic mouse non-muscle invasive bladder cancer model expressing the mammalian target of rapamycin signaling pathway. *J Korean Med Sci.* 2014;29(3):343–50.
 115. ScottL, Kruihof-De JulioM, PaoluzziL, KalacM, MarchiE, BuitragoJB, et al. Development and characterization of a novel CD19CherryLuciferase (CD19CL) transgenic mouse for the preclinical study of B-cell lymphomas. *Clin Cancer Res.* 2012;18(14):3803–11.
 116. PeterC, KielsteinJT, Clarke-KatzenbergR, AdamsMC, PitsiouniM, KambhamN, et al. A Novel Bioluminescent Tumor Model of Human Renal Cancer Cell Lines: An *In Vitro* and *In Vivo* Characterization. *J Urol.* 2007;177(6):2342–6.
 117. XuP, XuNJ, GuoK, XuAB, TakenakaF, MatsuuraE, et al. Real-time monitoring of tumor progression and drug responses in a preclinical mouse model of prostate cancer. *Oncotarget.* 2016;7(22):33025–34.
 118. LiuL, MasonRP, GimiB. Dynamic bioluminescence and fluorescence imaging of the effects of the antivascular agent Combretastatin-A4P (CA4P) on brain tumor xenografts. *Cancer Lett.* 2015;356(2, Part B):462–9.
 119. SanoD, ChoiS, MilasZL, ZhouG, GalerCE, SuY-W, et al. The effect of combination anti-endothelial growth factor receptor and anti-vascular endothelial growth factor receptor 2 targeted therapy on lymph node metastasis: a study in an orthotopic nude mouse model of squamous cell carcinoma of the oral tongue. *Arch Otolaryngol Head Neck Surg.* 2009;135(4):411–20.
 120. KurodaS, KubotaT, AoyamaK, KikuchiS, TazawaH, NishizakiM, et al. Establishment of a Non-Invasive Semi-Quantitative Bioluminescent Imaging Method for Monitoring of an Orthotopic Esophageal Cancer Mouse Model. *PLoS One.* 2014;9(12):e114562.
 121. L.D, X.Z, C.Y, T.Y, L.H, L.F, et al. Monitoring luciferase-labeled human prostate stem cell antigen-expressing tumor growth in a mouse model. *Exp Ther Med.* 2013;6(5):1208–12.
 122. SzentirmaiO, BakerCH, LinN, SzucsS, TakahashiM, KiryuS, et al. Noninvasive bioluminescence imaging of luciferase expressing intracranial U87 xenografts: Correlation with magnetic resonance imaging determined tumor volume and longitudinal use in assessing tumor growth and antiangiogenic treatment effect. *Neurosurgery.* 2006;58(2):365–72.
 123. ChoyG, O’ConnorS, DiehnFE, CostourosN, AlexanderHR, ChoykeP, et al. Comparison of noninvasive fluorescent and bioluminescent small animal optical imaging. *Biotechniques.* 2003;35(5):1022–30.
 124. ZabalaM, AlzugurenP, BenavidesC, CrettazJ, Gonzalez-AseguinolazaG, Ortiz de SolorzanoC, et al. Evaluation of bioluminescent imaging for noninvasive monitoring of colorectal cancer progression in the liver and its response to immunogene therapy. *Mol Cancer.* 2009;8:1–13.
 125. DincaEB, SarkariaJN, SchroederMA, CarlsonBL, VoicuR, GuptaN, et al. Bioluminescence monitoring of intracranial glioblastoma xenograft: response to primary and salvage temozolomide therapy. *J Neurosurg.* 2007;107(3):610–6.
 126. DicksonPV., HamnerB, NgCYC, HallMM, ZhouJ, HargrovePW, et al. *In vivo* bioluminescence imaging for early detection and monitoring of disease progression in a murine model of neuroblastoma. *J Pediatr Surg.* 2007;42(7):1172–

- 9.
127. JenkinsDE, YuSF, HornigYS, PurchioT, ContagPR. In vivo monitoring of tumor relapse and metastasis using bioluminescent PC-3M-luc-C6 cells in murine models of human prostate cancer. *Clin Exp Metastasis*. 2003;20(8):745–56.
128. NogawaM, YuasaT, KimuraS, KurodaJ, SatoK, SegawaH, et al. Monitoring luciferase-labeled cancer cell growth and metastasis in different in vivo models. *Cancer Lett*. 2005;217(2):243–53.
129. JenkinsDE, HornigYS, OeiY, DusichJ, PurchioT. Bioluminescent human breast cancer cell lines that permit rapid and sensitive in vivo detection of mammary tumors and multiple metastases in immune deficient mice. *Breast Cancer Res*. 2005;7(4):R444.
130. KemperEM, LeendersW, KüstersB, LyonsS, BuckleT, HeerschapA, et al. Development of luciferase tagged brain tumour models in mice for chemotherapy intervention studies. *Eur J Cancer*. 2006;42(18):3294–303.
131. JarzabekMA, HuszthyPC, SkafnesmoKO, McCormackE, DickerP, PrehnJHM, et al. In vivo bioluminescence imaging validation of a human biopsy-derived orthotopic mouse model of glioblastoma multiforme. *Mol Imaging*. 2013;12(3):161–72.
132. TerziyskaN, AlvesCC, GroissV, SchneiderK, FarkasovaK, OgrisM, et al. In Vivo Imaging Enables High Resolution Preclinical Trials on Patients' Leukemia Cells Growing in Mice. *PLoS One*. 2012;7(12):e52798.
133. ThalheimerA, KorbD, BönickeL, WiegeringA, MühlingB, SchneiderM, et al. Noninvasive visualization of tumor growth in a human colorectal liver metastases xenograft model using bioluminescence in vivo imaging. *J Surg Res*. 2013 Nov;185(1):143–51.
134. DerooseCM, ReumersV, GijsbersR, BormansG, DebyserZ, MortelmansL, et al. Noninvasive Monitoring of Long-Term Lentiviral Vector-Mediated Gene Expression in Rodent Brain with Bioluminescence Imaging. *Mol Ther*. 2006;14(3):423–31.
135. MollardS, FanciullinoR, GiacomettiS, SerdjabiC, BenzekryS, CiccoliniJ. In Vivo Bioluminescence Tomography for Monitoring Breast Tumor Growth and Metastatic Spreading: Comparative Study and Mathematical Modeling. *Sci Rep*. 2016;6:36173.
136. ChienY-C, ChenJC-H, LinW-C, DingH-J, WangH-E, KaoC-HK, et al. Using [18F]FBAU for imaging brain tumor progression in an F98/tk-luc glioma-bearing rat model. *Oncol Rep*. 2014;32(2):691–9.
137. WoolfendenS, ZhuH, CharestA. A Cre/LoxP conditional luciferase reporter transgenic mouse for bioluminescence monitoring of tumorigenesis. *Genesis*. 2009;47(10):659–66.
138. LinY-H, YangM-C, TsengS-H, JiangR, YangA, FarmerE, et al. Integration of Oncogenes via Sleeping Beauty as a Mouse Model of HPV16+ Oral Tumors and Immunologic Control. *Cancer Immunol Res*. 2018;
139. DayCP, CarterJ, BonomiC, HollingsheadM, MerlinoG. Preclinical therapeutic response of residual metastatic disease is distinct from its primary tumor of origin. *Int J Cancer*. 2012;130(1):190–9.

SUPPLEMENTARY TABLES

Table 1. Complete search strategy used in Ovid MedLine and EMBASE

MEDLINE

- 1 Luminescence/ (9152)
- 2 Luminescent Measurements/ (26882)
- 3 (bioluminescen* or luminescen* or "bioluminescent assay*" or "luminescen* measurement*" or "bioluminescen* measurement*" or "luminescent technique*" or BLI).tw,kf. (40289)
- 4 1 or 2 or 3 (62470)
- 5 cancer/ or malignancy/ or neoplasia/ or neoplasms/ or neoplasms, experimental/ or xenograft/ or heterograft/ or tumor/ (449760)
- 6 (cancer* or malignanc* or neoplasia or neoplasm* or tumor* or tumour* or xenograft* or heterograft*).tw,kf. (2792292)
- 7 5 or 6 (2874801)
- 8 Mice/ (1412662)
- 9 (mouse or mice or "laboratory mice" or "laboratory mouse" or "mus musculus domesticus").tw,kf. (1160238)
- 10 8 or 9 (1634623)
- 11 (correlat* or measur* or image* or imaging* or signal*).tw,kf. (5957362)
- 12 4 and 7 and 10 and 11 (2232)

EMBASE

- 1 bioluminescence/ (12412)
 - 2 luminescence/ (24319)
 - 3 (bioluminescen* or luminescen* or "bioluminescent assay*" or "luminescen* measurement*" or "bioluminescen* measurement*" or "luminescent technique*" or BLI).tw,kw. (42058)
 - 4 1 or 2 or 3 (53883)
 - 5 malignant neoplasm/ or neoplasm/ or tumor xenograft/ or xenograft/ or cancer/ or heterograft/ (681832)
 - 6 (cancer* or malignanc* or neoplasia or neoplasm* or tumor* or tumour* or xenograft* or heterograft*).tw,kw. (3874812)
 - 7 5 or 6 (3962073)
 - 8 mouse/ or murine/ or experimental mouse/ or mus musculus/ (1774371)
 - 9 (mouse or mice or "laboratory mice" or "laboratory mouse" or "mus musculus domesticus" or "experimental mouse" or "experimental mice").tw,kw. (1556057)
 - 10 8 or 9 (2002096)
 - 11 correlation analysis/ or correlation coefficient/ or measurement/ or imaging/ (549947)
 - 12 (correlat* or measur* or image* or imaging* or signal*).tw,kw. (7761033)
 - 13 11 or 12 (7820495)
 - 14 4 and 7 and 10 and 13 (4863)
-

Table 2. Summary of eligible publications included for analysis

Site of tumor	Local or metastatic	R ²	Tumor burden assessment	Clonal selection	Ref
OT	local	0.98	weight	no	(41)
OT	local	0.88	caliper	n/a	(42)
OT	local	0.92	caliper	n/a	(42)
OT	local	0.68	caliper	n/a	(42)
OT	local	0.94	caliper	n/a	(42)
OT	metastatic	0.93	weight	n/a	(43)
IP	local	0.99	caliper	no	(44)
IP	local	0.85	caliper	n/a	(44)
IP	local	0.97	caliper	n/a	(44)
OT	metastatic	0.96	caliper	n/a	(45)
OT	local	0.77	CT/MRI/PET/Ultrasound	n/a	(46)
OT	local	0.71	CT/MRI/PET/Ultrasound	n/a	(46)
OT	local	0.19	CT/MRI/PET/Ultrasound	n/a	(33)
OT	local	0.00	CT/MRI/PET/Ultrasound	n/a	(33)
OT	local	0.30	CT/MRI/PET/Ultrasound	n/a	(33)
OT	local	0.04	CT/MRI/PET/Ultrasound	n/a	(33)
OT	local	0.03	CT/MRI/PET/Ultrasound	n/a	(33)
OT	local	0.0001	CT/MRI/PET/Ultrasound	n/a	(33)
IV	metastatic	0.98	FACS	no	(25)
OT	local	0.93	weight	no	(47)
OT	local	0.99	weight	n/a	(48)
OT	local	0.99	caliper	n/a	(48)
OT	local	0.69	CT/MRI/PET/Ultrasound	no	(49)
SQ	local	0.93	caliper	n/a	(50)
OT	local	0.81	caliper	n/a	(35)
OT	local	0.79	weight	no	(51)
IV	metastatic	0.96	FACS	yes	(52)
IV	metastatic	0.95	FACS	yes	(52)
IP	metastatic	0.089	caliper	no	(21)
OT	local	0.77	ex vivo	n/a	(53)
OT	metastatic	0.66	ex vivo	n/a	(54)
SQ	local	0.76	caliper	no	(55)
OT	metastatic	0.73	weight	no	(56)
IP	metastatic	0.43	CT/MRI/PET/Ultrasound	yes	(57)
IV	metastatic	0.84	ex vivo	no	(58)
OT	local	0.76	CT/MRI/PET/Ultrasound	no	(59)
SQ	local	0.83	CT/MRI/PET/Ultrasound	no	(60)
OT	local	0.46	CT/MRI/PET/Ultrasound	no	(61)
OT	local	0.55	CT/MRI/PET/Ultrasound	no	(61)
OT	local	0.35	CT/MRI/PET/Ultrasound	no	(61)
OT	local	0.85	CT/MRI/PET/Ultrasound	yes	(62)
OT	local	0.88	CT/MRI/PET/Ultrasound	n/a	(34)
OT	local	0.42	CT/MRI/PET/Ultrasound	n/a	(34)
OT	local	0.14	CT/MRI/PET/Ultrasound	n/a	(34)

OT	local	0.54	CT/MRI/PET/Ultrasound	no	(63)
IP	metastatic	0.82	weight	yes	(64)
SQ	metastatic	0.78	caliper	yes	(64)
OT	local	0.93	caliper	no	(65)
IP	local	0.15	weight	yes	(66)
IP	metastatic	0.58	weight	yes	(66)
OT	local	0.94	caliper	yes	(67)
SQ	local	0.90	caliper	yes	(67)
SQ	metastatic	0.41	caliper	n/a	(68)
OT	local	0.80	CT/MRI/PET/Ultrasound	n/a	(69)
OT	local	0.94	weight	no	(70)
OT	local	0.81	CT/MRI/PET/Ultrasound	no	(37)
SQ	local	0.98	caliper	yes	(71)
IP	metastatic	0.80	CT/MRI/PET/Ultrasound	no	(30)
SQ	local	0.90	caliper	no	(72)
SQ	local	0.83	caliper	no	(73)
SQ	local	0.94	caliper	no	(74)
SQ	local	0.94	caliper	no	(74)
IV	metastatic	0.73	EPR	n/a	(15)
SQ	local	0.50	weight	n/a	(15)
SQ	local	0.42	weight	n/a	(15)
SQ	local	0.20	caliper	no	(75)
SQ	local	0.37	caliper	no	(76)
SQ	local	0.035	caliper	no	(76)
OT	local	0.81	caliper	n/a	(10)
SQ	local	0.72	caliper	n/a	(10)
SQ	local	0.97	caliper	yes	(4)
SQ	local	0.86	caliper	yes	(4)
SQ	local	0.85	caliper	yes	(4)
IV	metastatic	0.9	weight	yes	(4)
SQ	local	0.93	caliper	yes	(4)
SQ	local	0.88	caliper	yes	(4)
OT	local	0.97	weight	no	(77)
OT	local	0.99	caliper	no	(77)
spontaneous	local	0.77	weight	n/a	(78)
SQ	local	0.90	weight	yes	(79)
SQ	metastatic	0.99	caliper	no	(80)
IV	metastatic	0.99	weight	no	(80)
SQ	local	0.99	caliper	n/a	(81)
SQ	local	0.56	caliper	yes	(82)
SQ	local	0.86	caliper	yes	(82)
SQ	local	0.81	CT/MRI/PET/Ultrasound	no	(36)
OT	local	0.64	CT/MRI/PET/Ultrasound	no	(83)
SQ	local	0.92	caliper	n/a	(84)
SQ	local	0.37	caliper	n/a	(85)
SQ	local	0.12	caliper	n/a	(85)

SQ	local	0.094	caliper	n/a	(85)
OT	local	0.72	CT/MRI/PET/Ultrasound	n/a	(86)
OT	metastatic	0.13	weight	n/a	(87)
OT	metastatic	0.76	weight	n/a	(87)
SQ	local	0.67	caliper	yes	(88)
SQ	local	0.62	weight	no	(89)
IP	metastatic	0.93	CT/MRI/PET/Ultrasound	no	(90)
IP	metastatic	0.84	CT/MRI/PET/Ultrasound	no	(90)
SQ	local	0.63	caliper	no	(17)
SQ	local	0.41	caliper	no	(17)
SQ	local	0.93	caliper	no	(17)
IP	metastatic	0.92	weight	n/a	(91)
IP	metastatic	0.91	weight	n/a	(91)
OT	local	0.79	CT/MRI/PET/Ultrasound	n/a	(38)
SQ	local	0.99	caliper	n/a	(92)
IP	metastatic	0.98	CT/MRI/PET/Ultrasound	n/a	(93)
SQ	local	0.91	weight	no	(94)
SQ	local	0.74	weight	no	(94)
SQ	local	0.94	caliper	n/a	(95)
SQ	local	0.78	weight	no	(96)
OT	local	0.93	ex vivo	no	(97)
OT	local	0.95	Cavalieri serial slides	no	(97)
OT	local	0.65	caliper	no	(97)
OT	local	0.77	weight	no	(97)
OT	local	0.98	weight	no	(98)
OT	local	0.84	blood/urine	no	(99)
OT	local	0.55	blood/urine	no	(99)
OT	local	0.62	caliper	no	(99)
OT	local	0.63	caliper	no	(99)
OT	local	0.80	caliper	no	(99)
SQ	local	0.70	caliper	n/a	(100)
SQ	local	0.67	caliper	no	(100)
SQ	local	0.72	caliper	no	(100)
SQ	local	0.96	caliper	no	(19)
SQ	local	0.90	caliper	no	(19)
SQ	local	0.96	caliper	no	(19)
SQ	local	0.67	CT/MRI/PET/Ultrasound	no	(19)
SQ	local	0.38	CT/MRI/PET/Ultrasound	no	(19)
SQ	local	0.61	CT/MRI/PET/Ultrasound	no	(19)
SQ	metastatic	0.73	weight	no	(18)
SQ	metastatic	0.81	weight	no	(18)
SQ	metastatic	0.93	weight	no	(18)
SQ	metastatic	0.98	weight	no	(18)
OT	metastatic	0.91	FACS	no	(101)
OT	metastatic	0.98	ex vivo	no	(101)
OT	metastatic	0.9	weight	yes	(102)

SQ	local	0.94	caliper	no	(103)
IP	metastatic	0.74	weight	n/a	(104)
IP	local	0.76	CT/MRI/PET/Ultrasound	no	(105)
IP	local	0.82	CT/MRI/PET/Ultrasound	no	(105)
IP	local	0.93	CT/MRI/PET/Ultrasound	no	(105)
spontaneous	local	0.86	weight	n/a	(106)
SQ	local	0.71	caliper	no	(16)
SQ	local	0.065	caliper	no	(16)
SQ	local	0.86	caliper	n/a	(107)
SQ	local	0.90	caliper	n/a	(107)
SQ	local	0.90	caliper	n/a	(108)
OT	local	0.64	caliper	n/a	(109)
OT	local	0.92	weight	yes	(110)
OT	local	0.91	weight	yes	(110)
OT	local	0.90	weight	yes	(110)
OT	local	0.81	weight	yes	(110)
OT	local	0.71	caliper	yes	(111)
SQ	local	0.99	caliper	yes	(111)
IP	metastatic	0.59	weight	no	(112)
IP	metastatic	0.32	caliper	no	(112)
IP	metastatic	0.77	weight	yes	(113)
OT	local	0.87	weight	n/a	(114)
IP	metastatic	0.80	weight	n/a	(24)
spontaneous	metastatic	0.81	weight	n/a	(115)
SQ	local	0.36	weight	no	(116)
SQ	local	0.90	weight	yes	(117)
SQ	metastatic	0.90	blood/urine	yes	(117)
OT	metastatic	0.95	blood/urine	yes	(117)
SQ	local	0.86	caliper	yes	(118)
OT	local	0.97	caliper	no	(119)
SQ	local	0.92	caliper	yes	(120)
SQ	local	0.98	caliper	no	(121)
OT	local	0.54	CT/MRI/PET/Ultrasound	no	(122)
SQ	local	0.92	weight	no	(123)
SQ	local	0.97	caliper	no	(123)
IP	metastatic	0.41	CT/MRI/PET/Ultrasound	no	(124)
SQ	local	0.88	CT/MRI/PET/Ultrasound	no	(124)
IP	metastatic	0.84	CT/MRI/PET/Ultrasound	no	(124)
SQ	local	0.41	CT/MRI/PET/Ultrasound	no	(124)
IP	metastatic	0.42	ex vivo	no	(124)
OT	metastatic	0.94	caliper	no	(125)
SQ	local	0.73	caliper	no	(126)
OT	local	0.80	caliper	no	(126)
SQ	local	0.92	caliper	yes	(127)
SQ	local	0.90	caliper	yes	(127)
SQ	local	0.99	caliper	yes	(127)

OT	local	0.98	caliper	yes	(127)
SQ	local	0.96	caliper	yes	(128)
OT	local	0.74	CT/MRI/PET/Ultrasound	no	(31)
OT	local	0.56	CT/MRI/PET/Ultrasound	no	(31)
OT	local	0.58	CT/MRI/PET/Ultrasound	no	(31)
OT	local	0.83	CT/MRI/PET/Ultrasound	no	(31)
OT	local	0.46	CT/MRI/PET/Ultrasound	no	(31)
OT	metastatic	0.75	caliper	yes	(129)
OT	metastatic	0.99	caliper	yes	(129)
OT	metastatic	0.98	caliper	yes	(129)
OT	metastatic	0.97	caliper	yes	(129)
OT	local	0.53	ex vivo	no	(130)
OT	local	0.79	CT/MRI/PET/Ultrasound	no	(131)
IV	metastatic	0.74	FACS	no	(132)
IV	metastatic	0.42	FACS	no	(132)
IV	metastatic	0.74	CT/MRI/PET/Ultrasound	no	(32)
OT	metastatic	0.70	CT/MRI/PET/Ultrasound	yes	(32)
OT	Local	0.97	caliper	no	(133)
OT	Local	0.91	caliper	no	(133)
OT	Local	0.89	ex vivo	n/a	(134)
OT	Local	0.62	weight	n/a	(135)
SQ	local	0.91	caliper	no	(136)
OT	Local	0.98	caliper	n/a	(137)
Spontaneous	Local	0.69	caliper	n/a	(138)
SQ	Metastatic	0.80	weight	no	(139)
